DOI: 10.1021/ic100898g

Inorganic Chemistry
Article

Untypical $[VOPO_4]^-$ Layer in Vanadyl Phosphates with Variant Interlayer Gap of Double-Tiered Template

Ya-Ching Yang,[†] Yi-Chun Lai,[†] Joel R. Salazar,[‡,§] Vítězslav Zima,[∥] Kwang-Hua Lii,[‡] and Sue-Lein Wang*,[†]

[†]*Department of Chemistry, National Tsing Hua, Hsinchu 30013 Taiwan, Republic of China,* [‡]*Department of Chemistry, National Central University, Jhongli 32001, Taiwan, Republic of China,* [§]*Institute of Chemistry, University of the Philippines, Quezon City, Philippines , and* [∥]*Institute of Macromolecular Chemistry AS CR, v.v.i., Heyrovský Sq. 2, 16206, Prague 6, Czech Republic*

Received May 6, 2010

Four new organically templated layered vanadyl(IV) phosphates, (Hcha)$VOPO_4 \cdot 0.5H_2O$ (cha = cyclohexylamine) (**1**), (Hchpa)$VOPO_4 \cdot 0.5H_2O$ (chpa=cycloheptylamine) (**2**), $(Hcha)_{0.5}(Hchpa)_{0.5}VOPO_4 \cdot 0.5H_2O$ (**3**), and (H_2aepip)-$[(VOPO_4)_2(H_2O)] \cdot H_2O$ (aepip = *N*-(2-aminoethyl)piperazine) (**4**), have been synthesized under mild hydrothermal conditions and characterized by single-crystal X-ray diffraction, thermogravimetric analysis, magnetic susceptibility, and electron paramagnetic resonance (EPR) spectroscopy. They displayed a large interlayer gap propped up by an unprecedented double-tiered monoamine in vertical angles generating the lightest layered VPO material ever prepared and characterized. The anionic $[VOPO_4]^-$ sheets for all four compounds are constructed by a common secondary building unit consisting of one copper-acetate-type $\{(V^{IV}O)_2(\mu_2\text{-}PO_4)_4\}$ cluster and two vanadium polyhedra. The d^1 state was confirmed by both magnetic susceptibility studies and EPR spectra. Moreover, compounds **1** and **4** showed antiferromagnetism with T_N at 30 K, the highest ever observed in layered vanadyl phosphates. The structural relationship, template arrangement, magnetic property, thermal stability, and correlation between interlayer gaps and densities are discussed. Compounds **1**−**3** crystallized in the monoclinic space group $P2_1/c$ (no. 14) with $Z = 8$, whereas compound **4** crystallized in the orthorhombic space group *Pbca* (no. 61) with $Z = 4$. Crystal data of **1**, $a = 16.3461(9)$ Å, $b = 14.2641(8)$ Å, $c = 9.4037(5)$ Å, $\beta = 94.519(1)^o$, $V = 2185.8(2)$ Å^3; **2**, $a = 17.0773(5)$ Å, $b = 14.3449(4)$ Å, $c = 9.4251(3)$ Å, $\beta = 93.976(1)^o$, $V = 2303.3(1)$ Å^3; **3**, $a = 16.6765(4)$ Å, $b = 14.2927(3)$ Å, $c = 9.4120(3)$ Å, $\beta = 95.389(1)^o$, $V = 2233.5(1)$ Å^3; **4**, $a = 14.2517(9)$ Å, $b = 9.4012(6)$ Å, $c = 24.442(2)$ Å, $V = 3274.8(4)$ Å^3.

Introduction

Metal phosphates have been extensively studied due to their rich structural diversity[1] and potential applications in adsorption, ion exchange, electrical, and optical properties.[2] In this category, the system of layered vanadium phosphate in the general formula of $A_xVOPO_4 \cdot yH_2O$ (A = inorganic or organic cations) displays an extraordinary catalytic property, notable intercalation chemistry, and allows manifold redox reactions between layers.[3] With the various oxidation states and coordination environments (tetrahedral, square pyramidal, trigonal bipyramidal, and octahedral) of vanadium centers, numerous varieties of structural phases can be obtained by introducing diversified cations into the structure.[4] Discovering a flexible and significant inorganic matrix which can be propped up by different templates is a long quest in practical layered materials. Protonated organic amines between layers can act as counterparts for charge compensation and template agents to induce a larger layer gap. Two approaches are generally employed to augment interlayer space or porosity: (i) via large size polyamine molecules as templates to support the inorganic framework,[5] and (ii) via the moderate-size amine molecules comprising a

*Corresponding author. Fax: 886-35-711082. E-mail: slwang@mx.nthu.edu.tw.

(1) (a) Lii, K.-H.; Huang, Y.-F.; Zima, V.; Huang, C.-Y.; Lin, H.-M.; Jiang, Y.-C.; Liao, F.-L.; Wang, S.-L. *Chem. Mater.* **1998**, *10*, 2599–2609. (b) Cheetham, A. K.; Rao, C. N. R.; Feller, R. K. *Chem. Commun.* **2006**, 4780–4795. (c) Murugavel, R.; Choudhury, A.; Walawalkar, M. G.; Pothiraja, R.; Rao, C. N. R. *Chem. Rev.* **2008**, *108*, 3549–3655. (d) Natarajan, S.; Mandal, S. *Angew. Chem., Int. Ed.* **2008**, *47*, 4798–4829 .

(2) (a) Clearfield, A. *Mater. Chem. Phys.* **1993**, *35*, 257–263. (b) Clearfield, A. *Chem. Rev.* **1988**, *88*, 125–148. (c) Cheetham, A. K.; Férey, G.; Loiseau, T. *Angew. Chem., Int. Ed.* **1999**, *38*, 3268–3292. (d) Zhang, Y.; Tian, P.; Sun, Z.; Liu, Z.; Zhang, Y.; Qu, L.; Sang, S.; Liu, Z. *Solid State Commun.* **2007**, *141*, 407–411. (e) Maspoch, D.; Ruiz-Molina, D.; Veciana, J. *Chem. Soc. Rev.* **2007**, *36*, 770–818. (f) Feng, P. *Chem. Commun.* **2001**, 1668–1669. (g) Liao, Y.-C.; Lin, C.-H.; Wang, S.-L. *J. Am. Chem. Soc.* **2005**, *127*, 9986–9987. (h) Yang, Y.-C.; Wang, S.-L. *J. Am. Chem. Soc.* **2008**, *130*, 1146–1147. (i) Hung, S.-H.; Lin, C.-H.; Wu, W.-C.; Wang, S.-L. *Angew. Chem., Int. Ed.* **2009**, *48*, 6124–6127.

(3) (a) Gai, P. L; Kourtakis, K. *Science* **1995**, *267*, 661–663. (b) Centi, G.; Trifiro., F. *Chem. Rev.* **1988**, *88*, 55–80. (c) Ladwig, G. *Z. Anorg. Allg. Chem.* **1965**, *338*, 266.

(4) Boudin, S.; Guesdon, A.; Leclaire, A.; Borel, M.-M. *Int. J. Inorg. Mater.* **2000**, *2*, 561–579.

Published on Web 06/03/2010

well-defined hydrophobic part in the bilayer mode between inorganic sheets so as to create more space by van der Waals interaction.[6] The double-tier conformation, as only adopted by the second-type amine, was rarely reported in a MPO system.[7]

In our previous studies, large polyamines in different sizes were introduced into VPO layers to study template effects on interlayer separation.[5b] Besides molecule length, we observed that the inclined angle between organic template and inorganic sheet was another decisive factor. To further confirm and establish such template effects in pursuit of the lightest VPO materials, we have extended the choice of template to small monoamines instead of bulky polyamines. Thereupon, three new vanadyl(IV) compounds with untypical $[VOPO_4]^-$ anionic layer, $(HA)VOPO_4 \cdot 0.5H_2O$ (A = cha in **1**, chpa in **2**, and $(cha)_{0.5}(chpa)_{0.5}$ in **3**) with double tiers of templates residing vertically in the galleries were respectively synthesized by introducing cyclohexylamine (cha) and cycloheptylamine (chpa) separately or together. Among them, **2** has the largest interlayer spacing with the lowest density ever discovered, while **3** is the first example with two different organic templates in vanadium phosphates. As a comparison, a polyamine, aepip (*N*-(2-aminoethyl)piperazine), with a similar molecular shape but longer length than cha and chpa was subsequently used to prepare $(H_2A)[(VOPO_4)_2(H_2O)] \cdot H_2O$ (A = aepip) (**4**). As a result, the H_2aepip^{2+} was found to align in single-tier mode only, resulting in the shortest interlayer gap and the largest density in **4** among all four compounds. Comparing the arrangement of the shorter monoamines and the longer polyamine templates in compounds **1**−**4** led us to first discover that, instead of electrostatic force and hydrogen bonding, van der Waals interaction between neighboring molecules dominates the inclined angle of the monoamine. Herein, we report the syntheses, crystal structures, and properties of compounds **1**−**4**. Structural description and relationship, template distribution, thermal stability, magnetic property, and correlation between interlayer gaps and density are discussed in detail.

Experimental Section

Synthesis and Initial Characterization. Chemicals of reagent grade were used as received in the synthesis. Compounds **1**−**4** were synthesized under mild hydrothermal conditions using 23 mL Teflon-lined stainless steel vessels. The reactions were carried out at 180 °C under autogenous pressure for 3 days and followed by slow cooling at 6 °C·h^{-1} to room temperature. Green lamellar crystals of $(Hcha)VOPO_4 \cdot 0.5H_2O$ (**1**) were obtained from the reaction mixture of cha ($C_6H_{11}NH_2$, 4 mmol, 0.46 mL), KVO_3 (1 mmol, 0.138 g), vanadium powder (0.5 mmol, 0.026 g), H_3PO_4 (5 mmol, 0.35 mL), and H_2O (10 mL). The same reaction condition was used for the preparations of $(Hchpa)VOPO_4 \cdot 0.5H_2O$ (**2**) and $(Hcha)_{0.5}(Hchpa)_{0.5}VOPO_4 \cdot 0.5H_2O$ (**3**), with the amine replaced by chpa ($C_7H_{13}NH_2$, 4 mmol, 0.51 mL) for **2** and mixed cha (2 mmol, 0.23 mL) and chpa (2 mmol, 0.26 mL) for **3**. For compound **4**, $(H_2aepip)[(VOPO_4)_2(H_2O)] \cdot H_2O$ (aepip, $(HN(CH)_2N[(CH_2)NH_2](CH)_2$) was initially prepared under the same condition as compounds **1**−**3** with the monoamine substituted by aepip in half amount. A minor phase of green lamellar crystals was obtained. The optimized condition was later achieved by using V_2O_4 as the single source of vanadium and by decreasing the amount of amine to the molar ratio of A:V:P:H_2O = 3:1:6:660. Thereupon, larger green platelets of **4** were produced taking up 80% of the final product. The resulting products of all four compounds contained a major phase of green lamellar crystals suitable for single-crystal X-ray diffraction. However, all were contaminated with black unidentified particles embedded inside, which could be separated in **1** and **4** but much more difficult in **2** and **3**.

Scrupulously selected crystals of **1**−**4** were accumulated for thermogravimetric (TG) analysis. Only samples for **1** and **4** were collected in a sufficient amount for elemental analysis (EA), electron paramagnetic resonance (EPR), and superconducting quantum interference device (SQUID). The results of EA confirmed the stoichiometry of C, H, and N. Found/calcd (%) for **1**: C, 25.59/26.58; H, 5.83/5.58; N, 5.24/5.17 and for **4**: C, 14.51/14.67; H, 4.39/4.31; N, 9.09/8.56.

Single-Crystal X-ray Diffraction Analysis. Crystals of dimensions 0.200 × 0.200 × 0.125 mm for **1**, 0.300 × 0.300 × 0.025 mm for **2**, 0.200 × 0.150 × 0.025 mm for **3**, and 0.200 × 0.150 × 0.100 mm for **4** were selected for indexing and intensity data collection on a Bruker SMART APEX diffractometer equipped with a normal focus, 3 kW sealed X-ray source (λ = 0.71073 Å). Intensity data were collected at room temperature in 1271 frames with ω scans (width of 0.30° per frame). Unit cell dimensions were determined by a least-squares fit of 6633 reflections for **1**, 5716 reflections for **2**, 5557 reflections for **3**, and 7578 reflections for **4**. Empirical absorption corrections based on symmetry equivalents were applied (T_{min}/T_{max} = 0.952/0.860 for **1**, 0.957/0.832 for **2**, 0.948/0.772 for **3**, and 0.949/0.844 for **4**). On the basis of systematic absences and statistics of intensity distribution, the space groups were determined to be $P2_1/c$ for **1**−**3** and *Pbca* for **4.** The structures were solved by direct methods, with all nonhydrogen atoms located on electron density maps. Bond valence calculations indicated that the sites of O(11) (in **1**−**4**) and O(12) (in **4**) were water molecules. All counter species were clearly defined in the structure of **4**. However, in the case of **1**−**3**, water oxygen was found to display a static disorder on two sites, and thermal parameters of chpa molecules in **2** and **3** were comparatively large. All hydrogen (H) atoms on amine molecules were calculated on the basis of a riding model. The final cycles of refinement, including the atomic coordinates and anisotropic thermal parameters, for all nonH atoms and fixed atomic coordinates and isotropic thermal parameters for H atoms converged at $R1/wR2$ = 0.0469/0.1262 for **1**, 0.0408/0.1139 for **2**, 0.0418/0.1236 for **3**, and 0.0318/0.0879 for **4**. All calculations were performed using the PC version of the SHELXTL software package.[8] Crystallographic data are listed in Table 1, and the valence state for each vanadium site was determined based on its bond-valence sum (see Supporting Information, Table S1) and effective magnetic moment (vide infra). Selected bond distances and ORTEP drawings of **1**−**4** are given in the Supporting Information.

Magnetic Susceptibility and EPR Measurements. Variable-temperature magnetic susceptibility $\chi(T)$ were measured from 2 to 300 K in a magnetic field of 5 kG using a quantum design SQUID magnetometer on powder samples of **1** (21.1 mg) and **4** (14.8 mg). Corrections for diamagnetic contribution were made according to Selwood.[9] The magnetic data in the form of χ_M vs T and $\chi_M T$ vs T plots and $\chi_M{}^{-1}$ vs T were analyzed and fitted based on a Curie−Weiss behavior: $\chi_M = C/(T-\theta)$. Curie constant (C in

(5) (a) Liao, Y.-C.; Liao, F.-L.; Chang, W.-K.; Wang, S.-L. *J. Am. Chem. Soc.* **2004**, *126*, 1320–1321. (b) Yang, Y.-C.; Hung, L.-I.; Wang, S.-L. *Chem. Mater.* **2005**, *17*, 2833–2840. (c) Hu, L.; Fan, J.; Slebodnick, C.; Hanson, B. E. *Inorg. Chem.* **2006**, *45*, 7681–7688. (d) Jhang, P.-C.; Yang, Y.-C.; Lai, Y.-C.; Liu, W.-R.; Wang, S.-L. *Angew. Chem., Int. Ed.* **2009**, *48*, 742–745.

(6) (a) Yang, G. Y.; Sevov, S. C. *J. Am. Chem. Soc.* **1999**, *121*, 8389–8390. (b) Lin, C.-H.; Wang, S.-L. *Chem. Mater.* **2000**, *12*, 3617–3623. (c) Lai, Y.-L.; Lii, K.-H.; Wang, S.-L. *J. Am. Chem. Soc.* **2007**, *129*, 5350–5351.

(7) (a) Oliver, S.; Kuperman, A.; Lough, A.; Ozin, G. *Chem, Mater.* **1996**, *8*, 2391–2398. (b) Neeraj, S.; Natarajan, S. *J. Mater. Chem.* **2000**, *10*, 1171–1175. (c) Lin, C.-L.; Wang, S.-L. *Inorg. Chem.* **2001**, *40*, 2918–2921.

(8) Sheldrick, G. M. *Acta Crystallogr.* **2008**, *A64*, 112–122.

(9) Selwood, P. W. *Magnetochemistry*; Interscience: New York, 1956.

Table 1. Crystallographic Data for $(C_6H_{14}N)(VOPO_4)\cdot 0.5H_2O$ (**1**), $(C_7H_{16}N)(VOPO_4)\cdot 0.5H_2O$ (**2**), $(C_6H_{14}N)_{0.5}(C_7H_{16}N)_{0.5}(VOPO_4)\cdot 0.5H_2O$ (**3**), and $(C_6H_{17}N_3)[(VOPO_4)_2(H_2O)]\cdot H_2O$ (**4**)

	1	2	3	4
chemical formula	$C_6H_{15}NO_{5.5}PV$	$C_7H_{17}NO_{5.5}PV$	$C_{6.5}H_{16}NO_{5.5}PV$	$C_6H_{21}N_3O_{12}P_2V_2$
fw	271.10	285.13	278.11	491.11
a/Å	16.3461(9)	17.0773(5)	16.6765(4)	14.2517(9)
b/Å	14.2641(8)	14.3449(4)	14.2927(3)	9.4012(6)
c/Å	9.4037(5)	9.4251(3)	9.4120(3)	24.442(2)
β/°	94.519(1)	93.976(1)	95.389(4)	
V/Å^3	2185.2(2)	2303.3(1)	2233.5(1)	3274.8(4)
Z	8	8	8	4
space group	$P2_1/c$ (no. 14)	$P2_1/c$ (no. 14)	$P2_1/c$ (no. 14)	$Pbca$ (no. 61)
T/°C	23	23	23	23
λ(Mo Kα)/Å	0.71073	0.71073	0.71073	0.71073
ρ_{calcd}/g·cm^{-3}	1.648	1.644	1.654	2.008
data/restraints/parameters	5398/0/266	5724/47/294	5553/0/275	4074/0/227
μ(Mo Kα)/cm^{-1}	1.06	1.01	1.04	1.41
R_1[a]	0.0469	0.0408	0.0418	0.0318
wR_2[b]	0.1262	0.1139	0.1236	0.0879

[a] $R1 = \|F_o\| - |F_c\|/|F_o|$ for $F_o > 4\sigma(F_o)$. [b] $w = 1/[\sigma^2(F_o^2) + (aP)^2 + bP]$, $P = [Max(F_o) + 2(F_c)^2]/3$, where a/b = 0.0737/3.3969 for **1**, 0.0753/0.8326 for **2**, 0.0788/0.7847 for **3**, and 0.0583/0.0000 for **4**.

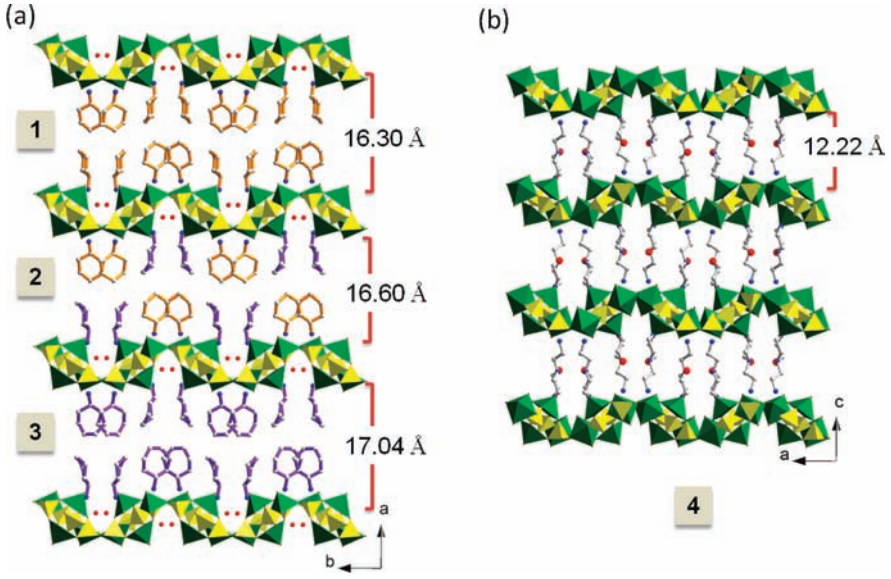

Figure 1. Structure plots for compounds **1**−**4**. (a) An integrated figure showing the identical inorganic layer with different composition of templates and interlayer distances of **1**−**3** (viewed toward the c axis). (b) Projection of compound **4** (viewed toward b axis). Green polyhedra for VO_5 in **1**−**3** and $VO_5(H_2O)$ in **4**. Yellow tetrahedra for PO_4. Orange molecule for cha, purple molecule for chpa. Red balls for O atoms in lattice water.

cm^3·K·mol^{-1}) and Weiss temperatures (θ in K) were respectively obtained: C = 0.347 and θ = −19.9 for **1**, and C = 0.701 and θ = −24.7 for **4**. X-band EPR spectra were recorded with a Bruker EMX-10 spectrometer between 4 and 300 K. The g values of these signals were measured relative to DPPH (g = 2.0036).

Thermogravimetric Analysis. Thermogravimetric analysis (TGA) using a Perkin-Elmer TGA-7 were performed on 1−3 mg powder samples under flowing N_2 with a heating rate of 10 °C·min^{-1}. As the TGA curves of all compounds indicate, the organic components were decomposed right after all lattice water molecules were removed. As shown in the Supporting Information, Figure S2, all the structures can sustain up to 250 °C. For compounds **1**−**4**, the total observed weight losses are in agreement with the calculated values (obs./calcd (%)): 42.4/43.2 for **1**, 44.8/46.0 for **2**, 42.9/43.7 for **3**, and 37.5/37.6 for **4**.

Results and Discussion

Structural Description and Relationship. Compounds **1**−**4** are vanadyl(IV) species adopting two-dimensional layered structures (Figure 1). The inorganic sheets consist of discrete VO_5 square pyramids and PO_4 tetrahedra. The secondary building unit (SBU) is constructed by one distinct binuclear vanadium motif and two mononuclear vanadium centers. As shown in Figure 2, the binuclear core consists of two VO_5 square pyramids with two axial V=O (the average V=O distance is 1.588 Å) pointing toward opposite directions and further links to four PO_4 groups in a bidentate mode forming a copper-acetate-like unit,[10] $\{(VO)_2(\mu_2\text{-}PO_4)_4\}$. It is rarely encountered in VPO systems and only documented in three compounds before, i.e., $(H_2tmdpp)(H_{1.5}tmdpp)K_{0.5}[V_5O_7(H_2O)_2(PO_4)_4]\cdot H_2O$ (tmdpp = 4,4′-trimethylenedipiperidine),[5b] $(H_4bappip)[(VO)_5(OH)_2(PO_4)_4]\cdot 2H_2O$ (bappip = 1,4-bis(aminopropyl)piperazine),[11a] and $[\{Cu\text{-}2(bisterpy)\}V_3O_5(HPO_4)_2(PO_4)]$ (bisterpy = 2,2′:4′,4″:2″,2‴-quarterpyridyl,6′,6″-dipyridine).[11b] Compared with them, this motif in **1**−**4** is

(10) Doedens, R. J. *Progress in Inorganic Chemistry v.21*; John Wiley & Sons, 1976, 209−231.

(11) (a) Soghomonian, V.; Chen, Q.; Zhang, Y.; Haushalter, R. C.; O'Connor, C. J.; Tao, C.; Zubieta, J. *Inorg. Chem.* **1995**, *34*, 3509–3519. (b) Koo, B.-K.; Ouellette, W.; Burkholder, E. M.; Golub, V.; O'Connor, C. J.; Zubieta, J. *Solid State Sci.* **2004**, *6*, 461–468.

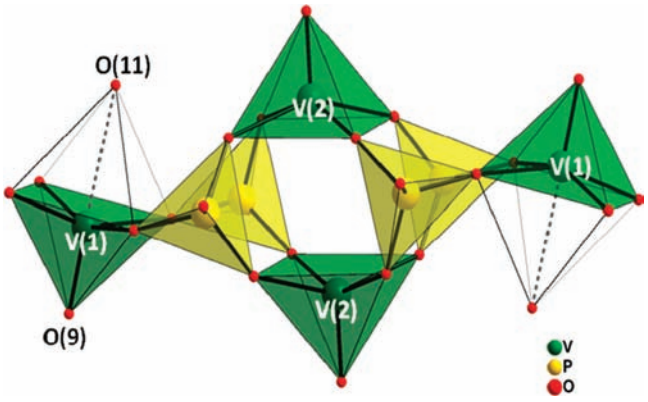

Figure 2. The secondary building unit, $\{(VO)_4(\mu_2\text{-}PO_4)_4\}$, of the inorganic layer in **1**−**4**. The water oxygen, O(11), may be viewed as the sixth ligand in **4**, as drawn in open face fashion.

laterally connected to two more VO_5 square pyramids through the phosphate groups forming the octameric SBU (Figure 2) that contains six four-membered rings. In the vicinity of each SBU, there is a lattice water, i.e., O(11), located close to the V(1) atom and trans to the terminal vanadyl V═O bond. The shortest distance between V(1) and O(11) in **1**−**3** is 2.530, 2.510, and 2.498 Å but in **4** it's 2.387 Å, falling within the range of coordination water reported in a VPO system.[12] Therefore, unlike their role as lattice water in **1**−**3**, we proposed that the O(11) in **4** can be considered as an aqua ligand complementing the sixth position of an VO_6 octahedron of V(1). Another lattice water O(12) in **4** is located between the layers without significant hydrogen bonding despite its close distance of 3.014 Å with a tertiary amino group, N(2).

As reported in literature, layered vanadium phosphates, $A_xVOPO_4 \cdot yH_2O$ (A = alkali or alkaline-earth metal), often share the common 4R inorganic sheet composed of corner-sharing VO_6 octahedra and PO_4 tetrahedra.[13] However, compounds **1**−**4** exhibit a novel polymorphic $VOPO_4$ layer with the same composition yet different connectivity and building units in this system. Through the symmetry operations of 2_1 screw axis along the *b* direction and *i* center in the middle of building unit, the SBUs are organized into a parquet-like pattern, as depicted in Figure 3a, forming an inorganic sheet with 4R and 6R windows. In compounds **1**−**3**, the corrugated layers on the *bc* plane are stacked in AAAA sequence along the [100] direction, where the water molecules reside in troughs and crests (Figure 1a). Each layer viewed toward the *a* axis is constituted by SBU connected into 4R chains, which are further linked via 6Rs to extend infinitely on the *bc* plane. Dissimilar to **1**−**3**, the two mononuclear vanadium units in SBUs of **4** are $VO_5(H_2O)$ octahedra with inorganic sheets on the *ab* plane constructed by 4R chains running along the *b* axis and the inorganic sheets changing the stacking sequence into an ABAB trend along the [001] direction (Figure 1b).

Template Arrangement. The organic templates in **1**−**3** have propped up interlayer spacing to 16.30, 17.03, and 16.60 Å, respectively (Figure 1). Between the layers, there are two distinct crystallographic sites for amine templates (Figure 3b): (i) the first site with a N(1) atom residing near the 6R window and forming hydrogen bonds with phosphate oxygens on the inorganic sheet (average N(1)···O = 2.847 Å);and (ii) the second site with a N(2) atom being slightly toward the trough and close to the water molecule (average distance of N(2)···O(11) = 2.683 Å, see the Supporting Information, Table S2). Notably, the selectivity of these two sites was observed in the mixed template compound **3** as the smaller $Hcha^+$ cations occupy the first site near the 6R window, while the bulkier $Hchpa^+$ reside on the second site seemed more suitable for larger templates. The spatial requirement for mix-templated **3** thus resulted in an intermediate layer gap between single-templated **1** and **2**. In **1**−**3**, the monoamine templates aligned in double tiered tail-to-tail mode with an average inclined angle of 87.8° (defined as the angle between a vector along the molecular extending length and the inorganic plane). It is the first time that monoamines are characterized to arrange into bilayer alignment, creating a hydrophobic region between the anionic VPO sheets. Noteworthy, that the zinc chlorophosphate of $[C_6NH_{14}][ZnCl(HPO_4)]$[7a] and aluminophosphate, UT-3,[7b] also exhibited such an unique bilayer packing of cyclo-aliphatic amine. However, their incline angles of amine molecules in these systems are only near 70° and 75°, pinned down by an anionic layer via strong hydrogen-bonding interaction. It is unusual to observe incline angles in **1**−**3** at almost 90°, as the organic templates stand upright giving larger interlayer spacing. In **4**, polyamine template, H_2aepip^{2+}, precludes the hydrophobic region allowing water molecules (O(12)) to be observed between the layers. The diprotonated aepip molecule acted as noncovalent-bonding pillars with an inclined angle around 80° with its primary amino group toward the 6R window and the secondary amino group on the piperazinyl ring close to the coordinated water of V(1). As the cyclic piperazine group in **4** is more hindered than the primary amino group in **1**−**3**, the nitrogen atom is more distant from the O(11) atom than from the primary amino groups in $Hcha^+$ or $Hchpa^+$ cations. Stronger attraction forces between O(11) and V(1) in **4** grant O(11) the role as a complementing aqua ligand of the sixth (octahedral) position coordinated to V(1) (Figure 2).

Magnetic, EPR, and Thermal Properties. Compounds **1**−**4** are considered a series because of the common structural features: four- and six-membered rings within two-dimensional (2D) anionic sheets formed of PO_4 tetrahedron, $V^{IV}O_5$ square pyramid, or $V^{IV}O_5(H_2O)$ octahedron. The $\{(VO)_2(\mu_2\text{-}PO_4)_4\}$ motif in **1** and **4** contains two $d^1(V^{IV})$ centers only 3.510 and 3.418 Å apart, respectively, leading to the observed antiferromagnetism (AFM). Plots of $\chi_M T$ vs T and $\chi_M{}^{-1}$ vs T are given in Figure 4. The AFM behavior was confirmed by a negative Weiss constant. Néel temperature, T_N, was observed

(12) (a) Loiseau, T.; Férey, G. *J. Solid State Chem.* **1994**, *111*, 416–421. (b) Bonavia, G.; DeBord, J.; Haushalter, R. C.; Rose, D.; Zubieta, J. *Chem. Mater.* **1995**, *7*, 1995–1998. (c) Harrison, W. T. A. *Solid State Sci.* **2003**, *5*, 297–302. (d) Huang, L.-H.; Lai, Y.-C.; Lai, H.-C.; Chiang, Y.-W.; Huang, J.-H.; Wang, S.-L. *Inorg. Chem.* **2009**, *48*, 11882–11888.

(13) (a) Wang, S.-L.; Kang, H.-Y.; Cheng, C.-Y.; Lii, K.-H. *Inorg. Chem.* **1991**, *30*, 3496–3499. (b) Kang, H.-Y.; Lee, W.-C.; Wang, S.-L.; Lii, K.-H. *Inorg. Chem.* **1992**, *31*, 4743–4748. (c) Papoutsakis, D.; Jackson, J. E.; Nocera, D. G. *Inorg. Chem.* **1996**, *35*, 800–801. (d) Roca, M.; Marcos, M. D.; Amorós, P.; Alamo, J.; Beltrán-Porter, A.; Beltrán-Porter, D. *Inorg. Chem.* **1997**, *36*, 3414–3421.

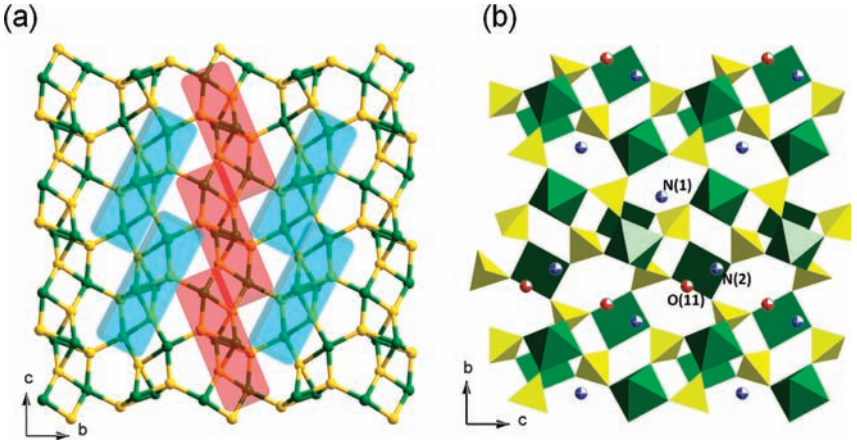

Figure 3. Section of the anionic $VOPO_4$ sheet in **1**−**4**. (a) Ball and stick drawing showing the parquet-like arrangement of the SBUs (shown in red or blue bricks). (b) Polyhedron plot along with projected position of the nitrogen atoms (in blue balls) of the amine molecules. Red balls are water oxygens.

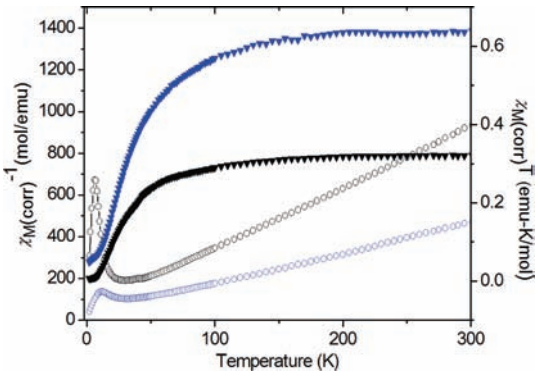

Figure 4. Temperature-dependent magnetic susceptibility data: plots of χ_M^{-1} vs T (○) and $\chi_M T$ vs T (▼). Curves for **1** are in black and for **4** in blue.

at 30 K for **1** and **4** (Supporting Information, Figure S3). To our knowledge, it is the highest T_N ever reported in a low-dimensional organically templated VPO system which is presumably induced by close V···V distance. Interestingly, as shown in Figure 4, an increase of χ_M^{-1} emerging at 6 K for **1** and 12 K for **4** may indicate a change of the magnetic structure at low temperature. Usually such a sharp increase of χ_M^{-1} at low temperature probably results from impurity. We suspect that the subtle change in the EPR spectra profile observed at 4 K for **1** and 10 K for **4** (Figure 5) indicates a possible change in magnetic dipole arrangement. The effective moments (μ_{eff}) per formula obtained for **1** and **4** were 1.67 and 2.37 μ_B, respectively, which matched with the spin-only value 1.73 μ_B for one d^1 center and 2.45 μ_B for two d^1 centers in formula. The EPR spectra of **1** at various temperatures displayed a single peak signal with an increasing line width from 300 to 4 K, inferring stronger dipole−dipole interaction with decreasing temperature. A similar trend was recorded on the EPR spectra of **4** with further hyperfine splitting observed at 4 K, which may arise from the closer distance between two V^{IV} centers in the $\{(VO)_2(\mu_2\text{-}PO_4)_4\}$ core and a different octahedral coordination environment of the lateral V(1) centers. The g value for compound **1** and **4** is 1.965 and 1.961, respectively.

From thermogravimetric analysis, with closely related structure features, compounds **1**−**3** displayed a similar weight loss of lattice water before ca. 150 °C, while **4** encountered an instant weight loss of lattice water upon heating before ca. 100 °C. The difference is attributed to the aforementioned insignificant hydrogen bonding between the lattice water and the inorganic sheet in **4**. All four structures would collapse on losing an organic amine, which decomposed right after all the lattice water was evacuated.

Template Effect Correlated with Density and Interlayer Gap. In controlling interlayer separation, molecule length and its inclined angle are crucial factors in the template effect, which is usually influenced by hydrogen bonding, charge interaction, and van der Waals force. For a polyamine, with more amino groups carrying positive charge, electrostatic force and hydrogen bonding are likely to dominate the extent of inclined angles of the template. Nevertheless, for monoamine, only the positively charged amonium side is attracted to the anionic inorganic layer, which allows the neutral hydrophobic side to drift between layers. The van der Waals interaction between neighbor organic templates becomes the only prevailing factor of the inclined angle. Moreover, larger d-spacing usually implies a lower density for the layered materials. As listed in Table 2, among the 15 reported 2D VPO compounds,[5b,14] $(H_2tmdpp)(H_{1.5}tmdpp)K_{0.5}[(V_5O_7)(H_2O)_2(PO_4)_4]\cdot H_2O$ displays the largest layer gap of 18.07 Å and the lowest density of 1.71 $g\cdot cm^{-3}$ with the longest diamine template tmdpp (~10.80 Å in length) and the largest inclined angle around 90°. However, due to the bilayer amine arrangement, we observed that the shorter monoamine chpa (~4.60 Å in length) could expand the layer gap to 17.03 Å with the density 1.64 $g\cdot cm^{-3}$ of **2**, an approximately 4% decrease from the record density. Figure 6 shows the distribution of densities vs interlayer distances of these layered VPOs which can be divided into three categories: the first includes structures that are not related and, hence, with no apparent correlation between density and d-spacing, as they are randomly distributed

(14) (a) Do, J.; Bontchev, R. P.; Jacobson, A. J. *J. Solid State Sci.* **2000**, *154*, 514–523. (b) Soghomonian, V.; Haushalter, R. C.; Zubieta, J. *Inorg. Chem.* **1994**, *33*, 1700–1704. (c) Bircsak, Z.; Harrison, W. T. A. *Inorg. Chem.* **1998**, *37*, 3204–3208. (d) Soghomonian, V.; Haushalter, R. C.; Zubieta, J.; O'Connor, C. J. *Inorg. Chem.* **1996**, *35*, 2826–2830. (e) Zima, V.; Lii, K.-H. *J. Solid State Sci.* **2003**, *172*, 424–430. (f) Cui, Y.; Sun, J.; Meng, H.; Li, G.; Chen, C.; Liu, Li; Yuan, X.; Pang, W. *Inorg. Chem. Commun.* **2005**, *8*, 759–762.

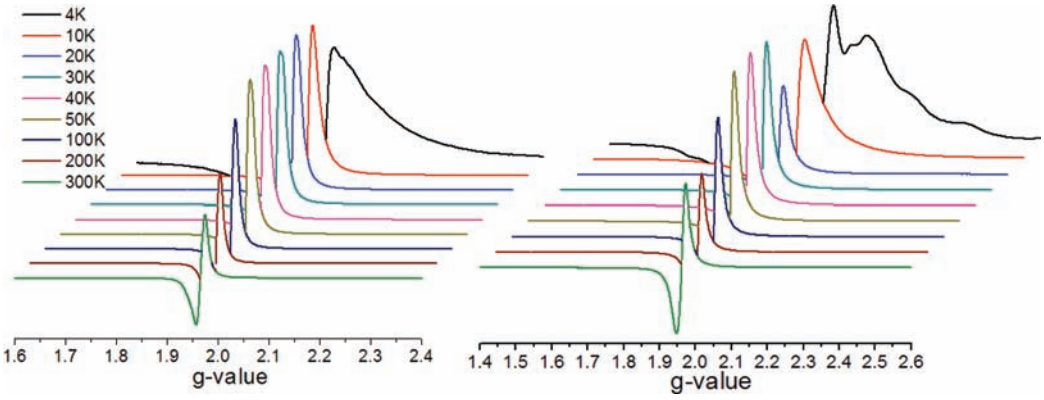

Figure 5. EPR spectra at various temperatures from 4 to 300 K for **1** (left) and **4** (right).

Table 2. Comparison in Interlayer d-Spacing, Density, And Template Arrangement for Layered VPO Structures

formula	d-spacing (Å)	density (g.cm^{-3})	template arrangement	ref
$[H_2pip][(VO)_4(OH)_4(PO_4)_2]$	10.011	2.497	ST[a]	14a
$(H_2pip)[(VO)(VO_2)_2(H_2O)(PO_4)_2]$	9.928	2.495	ST	14a
$[H_2dabco]_2(VO)_8(HPO_4)_3(PO_4)_4(OH)_2\cdot 2H_2O$	9.332	2.466	ST	11b
$(H_2dabco)[(VO)_3(OH)_2(PO_4)_2]$	9.771	2.397	ST	11b
$(H_2pip)[(VO)(PO_4)]_2$	8.198	2.359	ST	14b
$(CN_3H_6)_2(VO_2)_3(PO_4)(HPO_4)$	8.816	2.320	ST	14c
$(H_2pip)_2[(VO)_3(HPO_4)_2(PO_4)_2]\cdot H_2O$	7.316	2.280	ST	14d
$[H_2pip]_{1.5}[(VO)_2(HPO_4)_2(PO_4)]$	7.646	2.253	ST	14e
$(H_2en)_2[V_4O_6H(HPO_4)_2(PO_4)_2]$	11.653	2.212	ST	14e
$[H_4appip][(VO)_5(OH)_2(PO_4)_4\cdot 2H_2O$	8.586	2.159	ST	11b
$(H_2dach)_3[(VO)(V_2O_4)_2(PO_4)_4]\cdot 2H_2O$	9.871	1.869	ST	14f
$(H_3dien)[(VO)_2(OH)(PO_4)_2]\cdot H_2O$	7.750	2.115	ST	5b
$(H_2dach)_{1.5}[(VO)_2(OH)(PO_4)_2]\cdot 2H_2O$	10.581	1.804	ST	5b
$(H_2tmdpp)[(V_3O_4)(OH)(PO_4)_2]\cdot 3H_2O$	13.054	1.749	ST	5b
$(H_2tmdpp)(H_{1.5}tmdpp)K_{0.5}[(V_5O_7)(H_2O)_2(PO_4)_4]\cdot H_2O$	18.069	1.710	ST	5b
$(Hcha)(VOPO_4)\cdot 0.5H_2O$ (1)	16.295	1.648	DT[b]	this study
$(Hchpa)(VOPO_4)\cdot 0.5H_2O$ (2)	17.036	1.644	DT	this study
$(Hcha)_{0.5}(Hchpa)_{0.5}(VOPO_4)\cdot 0.5H_2O$ (3)	16.603	1.654	DT	this study
$(H_2aepip)[(VOPO_4)_2(H_2O)]\cdot H_2O$ (4)	12.221	2.008	ST	this study

[a] Amine template arranged as single-tiered. [b] Amine template arranged as double-tiered.

on the plot; the second group contains those with similar building units or amine templates, while their layer gaps increase and densities decrease with a longer amine length and a larger inclined angle; the ones included in the last group are compounds demonstrated in this study which reveals that the vertical double-tiered packing of monoamines can induce similar results like large polyamines on expanding the sheets. Furthermore, in contrast to cyclic monoamine in **1**−**3**, the larger polyamine (about 2 Å longer than cha and chpa), aepip, has comparable inclined angle (81°) but is arranged in single-tiered mode, bringing the structure of **4** the largest density of 2.01 g·cm^{-3} and the smallest d-spacing of 12.22 Å. Under the bilayer arrangement, we can further fine-tune the interlayer spacing by mixing two different monoamines providing the possibility to manipulate or design the space between layers.

In summary, four amine-templated vanadyl (IV) phosphates with new polymorphic $[VOPO_4]^-$ sheets have been prepared under mild hydrothermal conditions. Compounds **1**−**4** share a common building unit which can be arranged into a parquet-like pattern containing four- and six-membered rings. The space between the sheets is filled with different amine cations that display a bilayer (**1**−**3**) or a monolayer (**4**) arrangement, which substantially widens the interlayer gap from 12.22 to 17.03 Å. We made a breakthrough in generating the lightest layered

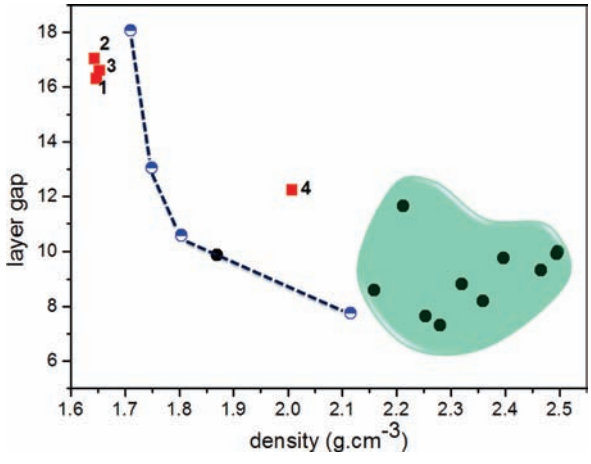

Figure 6. Schematic drawing showing the relationship between d-spacing and density for layered organic-templated VPO compounds. Red squares for **1**−**4** reported herein. Half-filled circles for VPOs in ref 5b. Filled circles for compounds prepared by other groups. Random distribution is indicated by the green area.

vanadyl phosphate with an untypical inorganic sheet and with an unique vertically double-tiered arrangement of organic monoamine templates between the layers. This study concludes that among the various possible controlling factors, van der Waals interaction solely contributes

to the vertically aligned monoamine template. Furthermore, we present the findings in that double tier of small monoamine is able to induce a larger interlayer gap than the single tier of bulkier polyamines and that a subtle adjustment of the d-spacing can be achieved with mixed organic templates.

Acknowledgment. We are grateful to the National Science Council of Taiwan for support of this work (97-2113-M-007-013-MY3). V.Z. wishes to thank the Czech Science Foundation (project no. 203/080208) for financial support.

Supporting Information Available: X-ray crystallographic information files (CIF), selected bond lengths and bond valence sums, table of possible hydrogen bonding, ORTEP drawings, TGA curves, and susceptibility (χ_M) versus T of **1**−**4.** This material is available free of charge via the Internet at http://pubs.acs.org.